Order and chaos in the rotation and revolution of a line segment and a point mass

John F. Lindner, Jacob Lynn, Frank W. King, and Amanda Logue
Physics Department, The College of Wooster, Wooster, Ohio 44691, USA
(Received 3 November 2009; revised manuscript received 10 January 2010; published 8 March 2010)

We study the classical dynamics of two bodies, a massive line segment or slash (/) and a massive point or dot (.), interacting gravitationally. For this slash-dot (/.) body problem, we derive algebraic expressions for the force and torque on the slash, which greatly facilitate analysis. The diverse dynamics include a stable synchronous orbit, generic chaotic orbits, sequences of unstable periodic orbits, spin-stabilized orbits, and spin-orbit coupling that can unbind the slash and dot. The extension of the slash provides an extra degree of freedom that enables the interplay between rotation and revolution. In this way, the slash-dot body problem exhibits some of the richness of the three body problem with only two bodies and serves as a valuable prototype for more realistic systems. Applications include the dynamics of asteroid-moonlet pairs and asteroid rotation and escape rates.

DOI: 10.1103/PhysRevE.81.036208 PACS number(s): 05.45.Pq, 95.10.Fh

I. INTRODUCTION

The three body problem [1–4] is of enduring importance to mathematical physics and celestial mechanics. It and related problems continue to inspire new and interesting research [5–11]. Increasing deep spaceflight activity and ongoing discoveries of extrasolar planets in unexpected orbits are some of the factors invigorating research in few body problems and celestial mechanics.

Recently discovered special cases of the three body problem include figure-8 orbits [9,10], in which three equal masses stably chase themselves around a closed trajectory resembling the numeral "8." Recent variations of the two body problem can exhibit chaos. For example, preserving Newton's second law but inverting Newton's third law converts the regular dynamics of the two body problem into chaotic dynamics [8]. Confining two bodies to a spherical universe results in arbitrarily complicated orbits due to the compact nature of the space [7]. Relaxing the traditional point mass approximations of the few body problem leads to the full body problem [11], in which the masses have arbitrary rotational inertias and experience net torques as well as net forces. Approximating Saturn's tiny, irregular satellite Hyperion as a dumbbell or gravitational dipole correctly models its chaotic tumbling [12,13].

In this paper, we study the gravitational interaction of a massive line segment or slash (/) and a massive point or dot (.). Predicting the motion of the Fig. 1 asteroids Ida and Dactyl is a natural, although approximate, example of such a slash-dot (/.) body problem. The slash-dot system is a simple but instructive prototype for the interplay between rotation and revolution, which characterize actual planets and natural satellites but not the interaction of idealized points. It is a semisolvable model problem in the vicinity of the famous two and three body problems that anchor celestial mechanics. For simplicity, we focus on the equal mass, planar slash-dot body problem, where initial conditions are constrained so that all motion is in a plane.

Despite being a perturbation of the simple two body problem, with one of the two points extended into a line segment, we demonstrate that the slash-dot body problem exhibits some of the richness of the three body problem. Its diverse dynamics include a strongly stable orbit, families of unstable periodic orbits, spin-stabilized nonchaotic orbits, and generic chaotic orbits, as in Fig. 2. Exploiting the system's extra degree of freedom, we show how angular momentum can flow from rotation to revolution and back, spinning up or spinning down the slash while decreasing or increasing its distance from the dot. Such angular momentum exchange can even unbind the slash and dot in situations where two dots would remain bound. Such orbits may be relevant to asteroid escape [15] and rotation rates [16].

Section II below derives an explicit algebraic formula for the gravitational potential energy of the slash-dot system and uses a Lagrangian approach to explicitly obtain the equations of motion. It expresses the forces and torques in terms of vectors and angles, and separately checks some special cases. Section III analytically and numerically generates qualitatively distinct kinds of orbits as a function of initial speed, spin, and slash length. It quantifies and visualizes these orbits in a variety of ways, including alignment per revolution and maximum Lyapunov exponent. Finally, it demonstrates the sometimes dramatic consequences of spin-orbit coupling. Section IV summarizes our results.

II. EQUATIONS OF MOTION

A. Coordinates

Relative to an arbitrary inertial origin $\mathcal{O}$, the point body or "dot" has mass m_d and position $\vec{r}_d$. The line body or "slash"

FIG. 1. (Color online) The asteroid Ida and its moonlet Dactyl form a natural slash-dot body system. (Photo credit: NASA/JPL.)

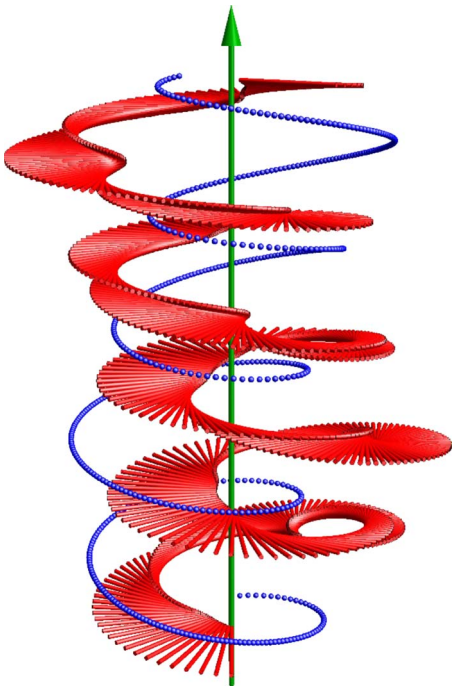

FIG. 2. (Color online) Strobed 2+1 dimensional spacetime evolution of the slash-dot system, for typical initial conditions and equal masses. Time increases upward (green arrow). Animations of the motion are available online [14]. By contrast, the corresponding motion of a two body system would form a regular double helix.

has mass m_s, length $\ell=2R$, orientation angle φ, and center $\vec{r}_s$ in the xy plane, as in Fig. 3. Relative to the system's center-of-mass $\mathcal{C}$ at

$$\vec{r}_c = \frac{m_s\vec{r}_s + m_d\vec{r}_d}{m_s + m_d}, \tag{1}$$

the slash and the dot are at

$$\vec{r}_{sc} = \vec{r}_s - \vec{r}_c = +\frac{\mu}{m_s}\vec{r}, \tag{2}$$

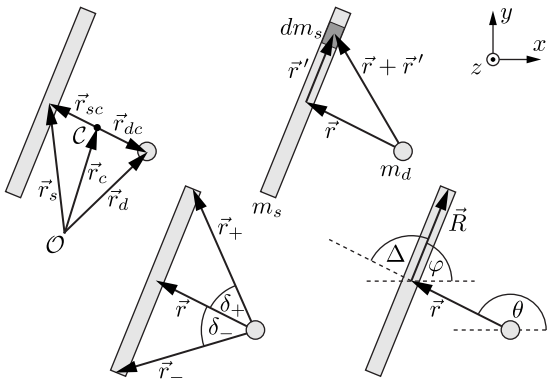

FIG. 3. Geometry for the slash-dot body problem. $\mathcal{O}$ is an arbitrary inertial origin and $\mathcal{C}$ is the system's center-of-mass.

$$\vec{r}_{dc} = \vec{r}_d - \vec{r}_c = -\frac{\mu}{m_d}\vec{r}, \tag{3}$$

where the reduced mass $\mu=m_sm_d/(m_s+m_d)$, and the displacement of the slash's center relative to the dot $\vec{r}=\vec{r}_s-\vec{r}_d$.

B. Potential energy

An infinitesimal length dr' of the slash has mass $dm_s=m_sdr'/\ell$ and location $\vec{r}'=\hat{x}r'\cos\varphi+\hat{y}r'\sin\varphi$ relative to the slash's center. Parameterize the relative displacement $\vec{r}=\hat{x}x+\hat{y}y$. Integrate over the slash's length to find the slash-dot potential energy

$$V = -\int_{-\ell/2}^{\ell/2}\frac{Gm_d}{|\vec{r}+\vec{r}'|}\frac{m_s}{\ell}dr' = -\frac{Gm_sm_d}{2R}\int_{-R}^{R}\frac{dr'}{\sqrt{(x+r'\cos\varphi)^2+(y+r'\sin\varphi)^2}}. \tag{4}$$

Complete the square in the denominator's radical and use a trigonometric substitution to find

$$V[\vec{r},\varphi] = V[x,y,\varphi] = -\frac{Gm_sm_d}{2R}\log\left[\frac{\sqrt{(x-R\cos\varphi)^2+(y-R\sin\varphi)^2}+R-x\cos\varphi-y\sin\varphi}{\sqrt{(x+R\cos\varphi)^2+(y+R\sin\varphi)^2}-R-x\cos\varphi-y\sin\varphi}\right]. \tag{5}$$

The potential exhibits the exact symmetries $V[\vec{r},\varphi]=V[-\vec{r},\varphi]$ and $V[\vec{r},\varphi]=V[\vec{r},\varphi+\pi]$. In terms of the Fig. 3 relative angle $\Delta=\theta-\varphi$ between the directed slash $\vec{R}$ and the relative displacement $\vec{r}$, the potential has the asymptotic expansion

$$V \sim -\frac{Gm_sm_d}{r}\left(1+\frac{1+3\cos[2\Delta]}{12}\left(\frac{R}{r}\right)^2\right). \tag{6}$$

At large distances $r\gg R$, the potential is approximately circularly symmetric and decays like the inverse of the distance, as in the classical two body problem. At small distances $r\sim R$, it conforms to the slash, as is illustrated in Fig. 4. In terms of the Fig. 3 vectors $\vec{r}_\pm=\vec{r}\pm\vec{R}$ from the dot to the slash's ends, the potential function simplifies to

$$V = -\frac{Gm_sm_d}{2R}\log\left[\frac{r_- - \hat{R}\cdot\vec{r}_-}{r_+ - \hat{R}\cdot\vec{r}_+}\right]. \tag{7}$$

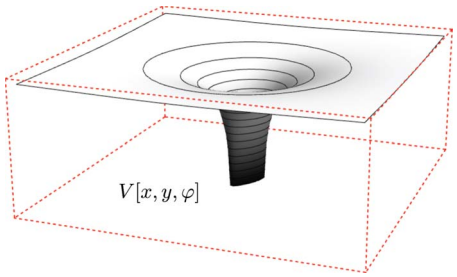

FIG. 4. (Color online) The slash-dot potential energy function V is approximately circular far from the slash but conforms to it nearby.

C. Kinetic energy

If the system's position is given by the relative coordinates x, y, and the rotation angle φ, then its relative velocity is $v_x=\dot{x}$, $v_y=\dot{y}$, and its spin angular velocity $\omega=\dot{\varphi}$, where the overdots indicate differentiation with respect to time. Relative to the arbitrary inertial origin $\mathcal{O}$, the dot and slash kinetic energies are

$$T_d = \frac{1}{2} m_d \dot{\vec{r}}_d^2, \tag{8}$$

$$T_s = \frac{1}{2} m_s \dot{\vec{r}}_s^2 + \frac{1}{2} I_s \dot{\varphi}^2, \tag{9}$$

where $I_s=m_s\ell^2/12=m_sR^2/3$ is the rotational inertia of the slash about its center (with the shorthand $\vec{v}^2=\vec{v}\cdot\vec{v}$). Relative to the system's stationary $\dot{\vec{r}}_c=\vec{0}$ center-of-mass, Eqs. (2) and (3) imply the total kinetic energy

$$\begin{aligned} T = T_d + T_s &= \frac{1}{2} m_d \dot{\vec{r}}_d^2 + \frac{1}{2} m_s \dot{\vec{r}}_s^2 + \frac{1}{2} I_s \dot{\varphi}^2 \\ &= \frac{1}{2} \mu \dot{\vec{r}}^2 + \frac{1}{2} I_s \dot{\varphi}^2 = T_{\mathcal{O}} + T_{\mathcal{S}}, \end{aligned} \tag{10}$$

where $T_{\mathcal{O}}=\mu\vec{v}^2/2$ is the orbital angular momentum and $T_{\mathcal{S}}=I_s\omega^2/2$ is the spin angular momentum.

D. Forces and torques

Extremizing the time integral of the Lagrangian $L=T-V$ produces the Euler-Lagrange equations of motion, which here reduce to Newton's equations

$$\vec{F} = \mu \ddot{\vec{r}} = \mu \dot{\vec{v}}, \tag{11}$$

$$\tau_z = I_s \ddot{\varphi} = I_s \dot{\omega}, \tag{12}$$

where the force's x component

$$\begin{aligned} \frac{\partial L}{\partial x} = F_x = \frac{G m_s m_d}{2R} & \frac{1}{y\cos\varphi - x\sin\varphi} \\ & \times \left(+ \frac{y + R\sin\varphi}{\sqrt{(x+R\cos\varphi)^2 + (y+R\sin\varphi)^2}} \right. \\ & \left. - \frac{y - R\sin\varphi}{\sqrt{(x-R\cos\varphi)^2 + (y-R\sin\varphi)^2}} \right), \end{aligned} \tag{13}$$

and the force's y component

$$\begin{aligned} \frac{\partial L}{\partial y} = F_y = \frac{G m_s m_d}{2R} & \frac{1}{y\cos\varphi - x\sin\varphi} \\ & \times \left(- \frac{x + R\cos\varphi}{\sqrt{(x+R\cos\varphi)^2 + (y+R\sin\varphi)^2}} \right. \\ & \left. + \frac{x - R\cos\varphi}{\sqrt{(x-R\cos\varphi)^2 + (y-R\sin\varphi)^2}} \right), \end{aligned} \tag{14}$$

and the torque's z component

$$\begin{aligned} \frac{\partial L}{\partial \varphi} = \tau_z = \frac{G m_s m_d}{8R} & \frac{1}{y\cos\varphi - x\sin\varphi} \\ & \times \left(- \frac{R^2 - (2x + R\cos\varphi)^2 - (2y + R\sin\varphi)^2}{\sqrt{(x+R\cos\varphi)^2 + (y+R\sin\varphi)^2}} \right. \\ & \left. + \frac{R^2 - (2x - R\cos\varphi)^2 - (2y - R\sin\varphi)^2}{\sqrt{(x-R\cos\varphi)^2 + (y-R\sin\varphi)^2}} \right). \end{aligned} \tag{15}$$

Because of Eqs. (2) and (3), the corresponding forces on the slash and the dot are

$$\vec{F}_s = m_s \ddot{\vec{r}}_{sc} = +\mu \ddot{\vec{r}} = +\vec{F}, \tag{16}$$

$$\vec{F}_d = m_d \ddot{\vec{r}}_{dc} = -\mu \ddot{\vec{r}} = -\vec{F}. \tag{17}$$

The force magnitude $F=\sqrt{F_x^2+F_y^2}$ has the asymptotic expansion

$$F \sim \frac{G m_s m_d}{r^2} \left(1 + \frac{1 + 3\cos[2\Delta]}{4} \left(\frac{R}{r} \right)^2 \right). \tag{18}$$

At large distances $r \gg R$, the force is approximately circularly symmetric and decays like the inverse square of the distance, as in the classical two body problem, but for small distances $r \sim R$, angular dependence corresponds to the slash's orientation. The torque decreases like the inverse cube of the distance and has the asymptotic expansion

$$\tau_z \sim - \frac{G m_s m_d}{2r^3} R^2 \sin[2\Delta]. \tag{19}$$

In terms of the Figs. 3 and 5 vectors $\vec{r}_\pm$ from the dot to the slash's ends, the force is

$$\vec{F} = \frac{G m_s m_d}{2Rr} \frac{\hat{z} \times (\hat{r}_+ - \hat{r}_-)}{\hat{z} \cdot \hat{r} \times \hat{R}}, \tag{20}$$

and hence is perpendicular to the line $\hat{r}_+ - \hat{r}_-$. The torque is

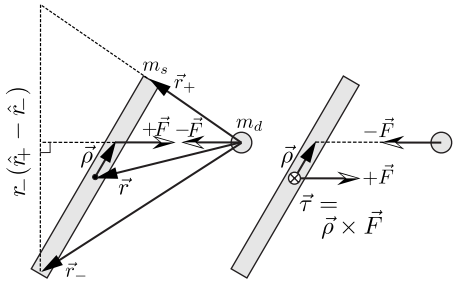

FIG. 5. Net forces are equal in magnitude and opposite in direction and perpendicular to the base of the constructed isosceles triangle. The force on the slash is effectively applied (left) opposite the force on the dot, where it naturally delivers the appropriate torque (right).

$$\vec{\tau} = -\frac{Gm_s m_d}{2R} \frac{\hat{r} \cdot (\hat{r}_+ - \hat{r}_-)}{\hat{z} \cdot \hat{r} \times \hat{R}} \hat{z}, \tag{21}$$

and is perpendicular to the xy plane, which contains all the motion. Since $\vec{r}$ is in the xy plane, $\vec{r} \cdot \hat{z} = 0$ and so

$$\vec{\tau} = -\frac{Gm_s m_d}{2Rr} \frac{\vec{r} \cdot (\hat{r}_+ - \hat{r}_-)\hat{z} - \vec{r} \cdot \hat{z}(\hat{r}_+ - \hat{r}_-)}{\hat{z} \cdot \hat{r} \times \hat{R}}$$
$$= -\frac{Gm_s m_d}{2Rr} \frac{\vec{r} \times [\hat{z} \times (\hat{r}_+ - \hat{r}_-)]}{\hat{z} \cdot \hat{r} \times \hat{R}} = -\vec{r} \times \vec{F} = \vec{\rho} \times \vec{F}, \tag{22}$$

as if the force on the slash due to the dot were applied locally a displacement $\vec{\rho}$ from the slash's center, as illustrated in Fig. 5. In terms of the Fig. 3 subtending angles $\delta_\pm$ and the relative angle $\Delta = \theta - \varphi$, the force magnitude is

$$F = \frac{Gm_s m_d}{Rr} \left| \frac{\sin[(\delta_+ + \delta_-)/2]}{\sin \Delta} \right|, \tag{23}$$

and the torque magnitude is

$$\tau = \frac{Gm_s m_d}{R} \left| \frac{\sin[(\delta_+ + \delta_-)/2] \sin[(\delta_+ - \delta_-)/2]}{\sin \Delta} \right|$$
$$= rF \left| \sin[(\delta_+ - \delta_-)/2] \right|. \tag{24}$$

Figure 6 illustrates how the force and torque components vary with the orientation of the slash. The transverse force $F_\perp$ and the torque τ_z vanish by symmetry when the slash is parallel ($\Delta = 0$ or $\Delta = \pi$) or perpendicular ($\Delta = \pi/2$ or $\Delta = 3\pi/2$) to the displacement vector $\vec{r}$ connecting the dot to the slash's center. Elsewhere, because the gravitational force decreases faster than linear, contributions due to the near end of the slash dominate contributions from the far end, resulting in nonzero transverse force and torque.

E. Parallel and perpendicular

When the slash is parallel to the vector $\vec{r}$ joining the slash's center to the dot, so that the slash points directly at the dot, the slope of the slash equals the slope of the relative displacement, $\tan \varphi = y/x$ so that $x \sin \varphi = y \cos \varphi$, and the

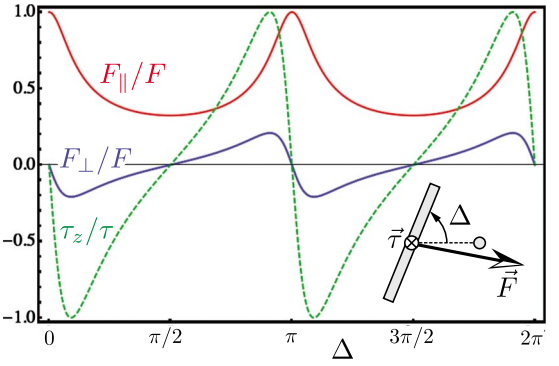

FIG. 6. (Color online) Normalized force and torque on a slash due to a dot, when the dot is just outside the range of an equally massive slash (inset), through one rotation of the slash.

denominators of the Eqs. (13)–(15) formulas for force and torque vanish. Fortunately, the numerators vanish also, and L'Hôpital's rule resolves the indeterminacy. For example, define the denominator factor $D = y \cos \varphi - x \sin \varphi$ and the numerator factor $N = F_x D$ and evaluate

$$F_{x,\parallel} = \lim_{\tan \varphi \to y/x} \frac{N}{D} = \lim_{\tan \varphi \to y/x} \frac{\partial N/\partial \varphi}{\partial D/\partial \varphi} = -\frac{Gm_s m_d}{r^2 - R^2} \frac{x}{r}. \tag{25}$$

Thus,

$$\vec{F}_\parallel = -\frac{Gm_s m_d}{r^2 - R^2} \hat{r}, \tag{26}$$

which can be verified by directly integrating the force in the pointing condition (with $r > R$ so the slash and the dot do not intersect). The limit $R \to 0$ recovers the expected force between two massive points; otherwise, the force is *larger* because the mass in the near half of the slash contributes more than the mass in the far half of the slash, as gravity decreases faster than linear.

When the slash is perpendicular to the vector $\vec{r}$ joining the slash's center to the dot, by direct integration, the force is

$$\vec{F}_\perp = -\frac{Gm_s m_d}{r\sqrt{r^2 + R^2}} \hat{r}. \tag{27}$$

Again, the limit $R \to 0$ recovers the expected force between two massive points; otherwise, the force is *smaller* because almost all of the slash is farther from the dot than the slash's center.

III. SOLUTIONS

A. Analytic special cases

The dot can hover over the end or midpoint of the slash if the dot revolves and the slash rotates at the appropriate frequency. To hover over the end of the slash (at a distance $r > R$), $F_\parallel = \mu r \omega_\parallel^2$ implies the frequency

$$\omega_\parallel = \frac{v_\parallel}{r} = \sqrt{\frac{G(m_s + m_d)}{r(r^2 - R^2)}}. \tag{28}$$

To hover over the midpoint of the slash (at any $r > 0$), $F_\perp = \mu r \omega_\perp^2$ implies the frequency

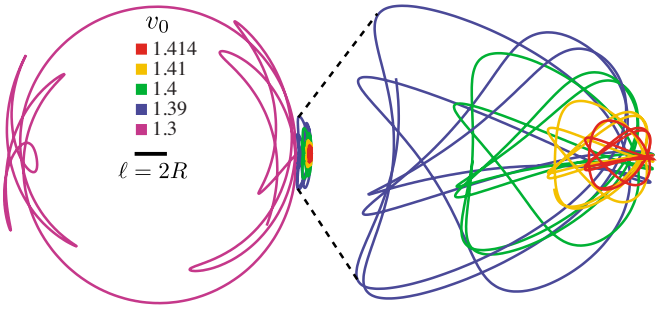

FIG. 7. (Color online) Successively larger perturbations of synchronous, stable, gravity-gradient $v_0=\sqrt{2}$, orbit of dot hovering over slash end (left) with an enlargement (right), in the slash's noninertial reference frame. Other parameters are $r_0=1$, $\omega_0=\sqrt{2}$, $\ell=0.2$, $m_s=1$, $m_d=1$.

$$\omega_\perp = \frac{v_\perp}{r} = \sqrt{\frac{G(m_s+m_d)}{r^2\sqrt{r^2+R^2}}}. \tag{29}$$

Perturbations of these synchronous orbits result in precession, as illustrated in Fig. 7, until the orbits become too large and wander chaotically.

B. Fiducial orbit

For simplicity, assume slash and dot have equal masses, $m_s=m_d\equiv m_\odot/2$ so that the total mass $m_s+m_d=m_\odot$. In the limit of vanishing length $\ell\to 0$, slash and dot orbit in a fiducial circle of diameter $d_\odot$ and *relative* speed

$$v_\odot = \sqrt{\frac{Gm_\odot}{d_\odot}}. \tag{30}$$

Relative escape speed from such a system is

$$v_e = \sqrt{\frac{2Gm_\odot}{d_\odot}} = \sqrt{2}v_\odot. \tag{31}$$

Reference results to these scales.

C. Collision approximation

If slash and dot are released with too little relative speed (and hence too little orbital angular momentum), they will collide. For small slash length, approximate this collision speed by assuming launch at apoapsis and collision at periapsis. In the limit of vanishing length $\ell\to 0$, conservation of energy implies

$$\frac{1}{2}\mu v_0^2 - \frac{G\mu(m_s+m_d)}{r_0} = \frac{1}{2}\mu v^2 - \frac{G\mu(m_s+m_d)}{r} \tag{32}$$

and conservation of angular momentum implies

$$\mu r_0 v_0 = \mu r v. \tag{33}$$

These conservation laws and Eq. (31) with $d_\odot=r_0$ imply

$$r = \frac{r_0}{2v_\odot^2/v_0^2 - 1} = \frac{r_0}{v_e^2/v_0^2 - 1} \tag{34}$$

at periapsis. If impact occurs when $r=\ell/2=R$, then the initial speed for collision is

$$v_0 = \frac{v_e}{\sqrt{1+2r_0/\ell}} = \frac{\sqrt{2}v_\odot}{\sqrt{1+r_0/R}} \equiv v_c. \tag{35}$$

Figures 9–11 plot the collision speed v_c as dashed lines demonstrating it to be a good approximation for small slash lengths and short times.

D. Numerical general cases

The Eqs. (11) and (12) equations of motion are nonlinear with arbitrarily complicated solutions. To further study them, we numerically integrate the equations for a wide range of parameters and initial conditions.

For smooth, nonstiff solutions where the functions (like our complicated forces and torques) are expensive to evaluate, and when precision is important, Adams-Moulton linear multistep integration methods are an excellent choice [17]. Our implementation utilizes the CVODE code [18]. We check this integration using a symplectic partitioned Runge-Kutta algorithm, which preserves the phase space structure of our Hamiltonian system. Our implementation uses the *Mathematica* NDSolve function [19]. Both algorithms are in excellent agreement, and very accurately conserve both energy and angular momentum. As an example, for our online animations [14], our integration algorithms conserve energy to about one part per million, $\Delta E/E\sim 10^{-6}$, and conserve angular momentum to about 100 parts per billion, $\Delta L/L\sim 10^{-7}$.

For speed and accuracy, we scale our variables so that the numerical value of the gravitational constant is unity, $G=1$. We focus on the equal mass case, scaled so that both the slash and dot masses are unity, $m_s=1$ and $m_d=1$. Finally, we scale our lengths so the initial separation of the slash and dot is also unity, $r_0=1$. With this scaling, the Sec. III B fiducial speeds for circular orbit and escape become $v_\odot=\sqrt{2}$ and $v_e=2$.

Figure 8 illustrates two (unstable) periodic orbits and one chaotic orbit, in the slash's noninertial reference frame, where a single curve well summarizes the entire motion. Hues code time along the dot's orbit and the horizontal black line segment indicates the slash. Note how a small change in initial condition of just one part in a thousand causes the chaotic orbit to radically diverge in less than 2 revolutions. Such extreme sensitivity to initial conditions is a hallmark of chaos.

To help study the relationship between rotation (spin of slash about its center) and revolution (orbit of slash and dot), define the alignment

$$\mathcal{A} = \hat{r}\cdot\hat{\ell} = \cos\Delta = \cos[\theta-\varphi], \tag{36}$$

where the Fig. 3 angles $\Delta=\theta-\varphi$ code the spin of the slash and the orbit of the system. The alignment $\mathcal{A}=\pm 1$ when the slash, thought of as a directed line segment, is pointing either toward (aligned) or away (antialigned) from the dot. The alignment $\mathcal{A}=0$ when the slash is perpendicular to the line joining the slash's center and the dot, and therefore pointing neither toward nor away from the dot.

Figures 9–11 plot alignment $\mathcal{A}$ (red-white-blue colors) as a function of initial speed v_0, initial spin ω_0, and slash length $\ell=2R$, in two different cross sections, after 1, 2,

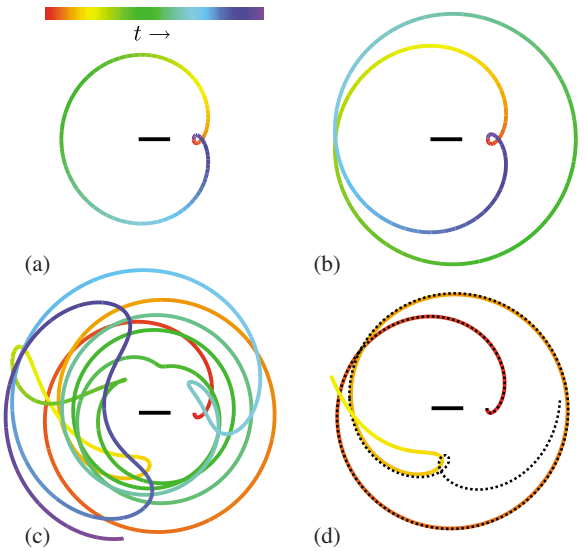

FIG. 8. (Color online) Periodic and chaotic orbits in the slash's noninertial reference frame. Initial speed $v_0=1.738\,81$ in (a) and $v_0=1.779\,83$ in (b) begin periodic orbits, while $v_0=1.8$ in (c) begins a chaotic orbit. Initial speed of dashed black orbit in (d) is just one part in a thousand larger than in (c), which causes these orbits to radically diverge in less than 2 revolutions. Hues code time along dot's orbit; black line indicates slash. Other parameters are $r_0=1$, $\omega_0=\sqrt{2}$, $\ell=0.8$, $m_s=1$, $m_d=1$. The corresponding motion of a two body system would form an ellipse centered on a dot.

and 4 revolutions. A revolution is the numerically computed time between successive periapses (minimum separations) or apoapses (maximum separations), depending on whether or not the initial condition is at periapsis or apoapsis. The slash begins pointed at the dot, with $\varphi_0=\pi/2$, as in the Fig. 9 inset.

In Fig. 9, the alignment spin-speed $\{\omega_0,v_0\}$ cross section (left) is at a length of $\ell=0.25$, and the length-speed $\{\ell,v_0\}$ cross section (right) is at a spin of $\omega_0=\sqrt{2}$. Banana (pale yellow) represents collisions, which naturally dominate for large slash lengths and small initial speeds. The dark blue "valley of stability" near the Eq. (28) $v_\parallel$ dotted line is where the gravity gradient stabilizes the dot hovering over one end of the slash in a synchronous orbit. Striped patterns at large positive or negative spins are spin-stabilized regular motions. Figure 10 indicates how the alignment landscape evolves in time, developing progressively finer features, while the inset to Fig. 11 suggests fractal-like structure that is consistent with extreme sensitivity to initial conditions and chaos.

In Fig. 9, the sequences of black triangles and disks represent distinct families of periodic orbits. Figure 12(a) depicts the triangle family with both fading strobe plots and plots of alignment $\mathcal{A}$ and separation r as a function of time. The minimum and maximum separations are the periapses and apopses. As the alignment varies between ±1, we fill the time trace with red or blue to emphasize the alignment reversals. Each successive orbit contains an extra rotation per revolution (spin per orbit). The triangle sequence is at constant slash length ℓ and forms a geometric series in initial speed v_0 accumulating to the escape speed v_e, where the period of the orbit (and hence the number of rotations per revolution) diverges to infinity.

Figure 12(b) depicts the disk family, where both slash length ℓ and initial speed v_0 vary. Again, each successive orbit contains an extra rotation per revolution. Such families of closed orbits can be discovered numerically by successive approximations using, for example, the Newton-Raphson method [17].

E. Lyapunov exponents

For each phase space dimension of a dynamical system, a Lyapunov exponent characterizes the exponential rate of

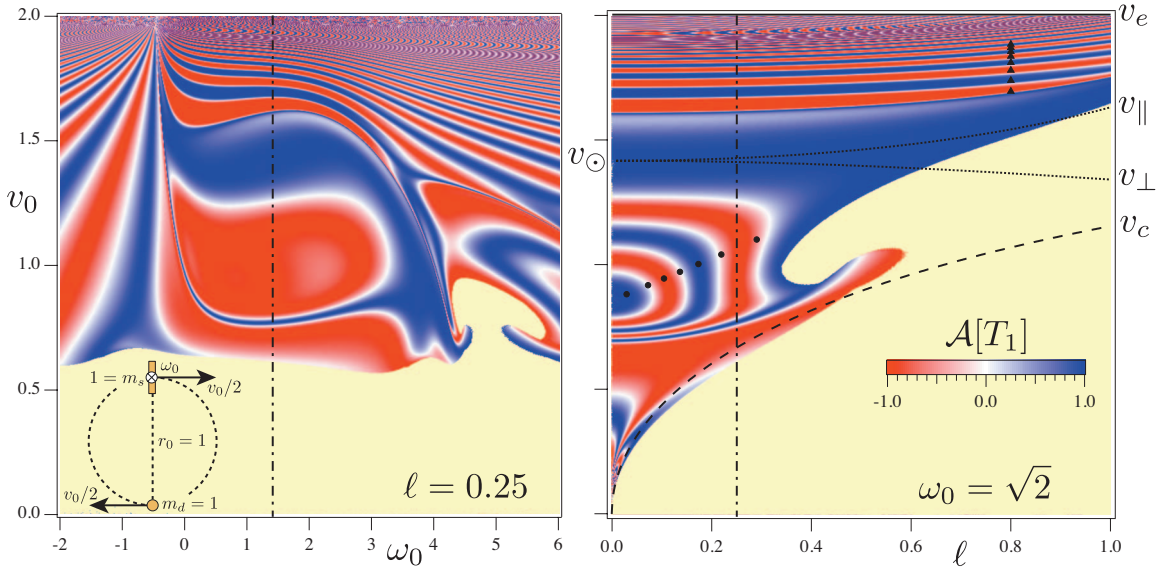

FIG. 9. (Color) Alignment $\mathcal{A}$ after 1 revolution of time T_1 (red-white-blue colors) as a function of initial speed v_0, initial spin ω_0, and slash length $\ell=2R$. Spin-speed $\{\omega_0,v_0\}$ cross section (left) is at a length of $\ell=0.25$; inset illustrates the initial conditions. Length-speed $\{\ell,v_0\}$ cross section (right) is at a spin of $\omega_0=\sqrt{2}$. Banana (pale yellow) represents collisions. Black disks and triangles (right) represent distinct families of periodic orbits. Vertical dot-dash lines indicate the intersection of the two plots.

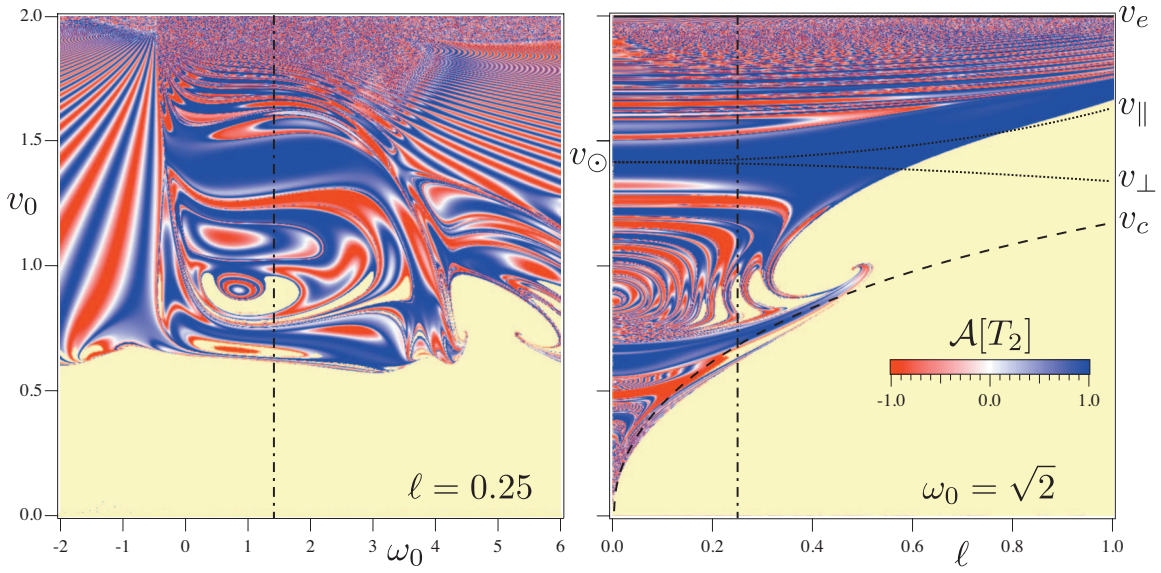

FIG. 10. (Color) Alignment $\mathcal{A}$ after 2 revolutions of time T_2 (red-white-blue colors) as a function of initial speed v_0, initial spin ω_0, and slash length ℓ. Other parameters as in Fig. 9. Vertical dot-dash lines indicate the intersection of the two plots.

separation of infinitesimally close initial conditions. One Lyapunov exponent is zero because nearby initial conditions along the same orbit never diverge. In order to preserve phase space volume in Hamiltonian systems, the Lyapunov exponents come in pairs that sum to zero [20], including one double zero. Since the (planar) slash-dot system is an autonomous Hamiltonian system of 3 degrees of freedom (relative displacement x, y, and slash orientation φ), which therefore occupies a six-dimensional phase space, its Lyapunov spectrum has the form $\{-\lambda,-\lambda',0,0,+\lambda',+\lambda\}$.

A positive largest Lyapunov exponent $\lambda>0$ indicates chaos. Since any initial separation vector will typical contain a component in the direction associated with the largest Lyapunov exponent, its exponential growth will dominate that of the other exponents. We estimate the largest Lyapunov exponent for the slash-dot system by integrating the corresponding variational equations.

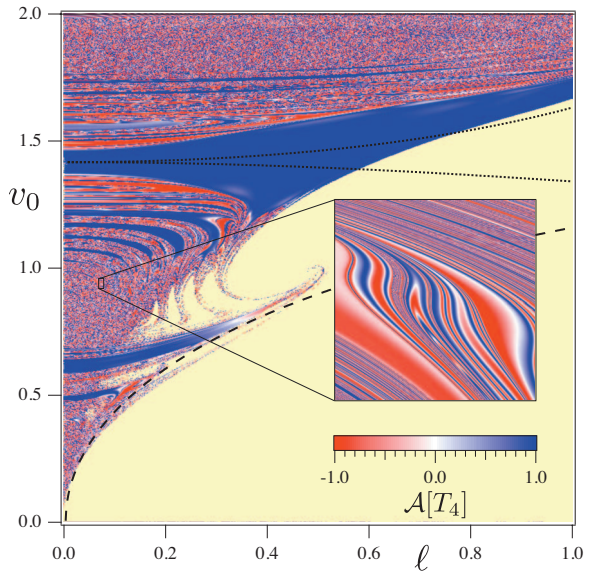

FIG. 11. (Color) Alignment $\mathcal{A}$ of system (red-white-blue colors) after 4 revolutions of time T_4 as a function of slash length ℓ and initial speed v_0. Closeup (inset) hints at fractal-like structure.

Let the slash-dot state be the abstract position vector $\mathcal{X}=\{x,y,\varphi,v_x,v_y,\omega\}$ and define the abstract velocity vector $\mathcal{V}=\{v_x,v_y,\omega,F_x/\mu,F_y/\mu,\tau_z/I_s\}$, so the Eqs. (11) and (12) equations of motion become

$$\frac{d\mathcal{X}}{dt}=\mathcal{V},\quad \lim_{t\to 0}\mathcal{X}=\mathcal{X}_0. \tag{37}$$

Differentiate both sides with respect to the initial conditions $\mathcal{X}_0$ to get the matrix-valued, linearized, variational equations [21].

$$\frac{d}{dt}\frac{\partial\mathcal{X}}{\partial\mathcal{X}_0}=\frac{\partial\mathcal{V}}{\partial\mathcal{X}}\cdot\frac{\partial\mathcal{X}}{\partial\mathcal{X}_0},\quad \lim_{t\to 0}\frac{\partial\mathcal{X}}{\partial\mathcal{X}_0}=I, \tag{38}$$

where I is the 6×6 identity matrix. Note that

$$\delta\mathcal{X}=\frac{\partial\mathcal{X}}{\partial\mathcal{X}_0}\cdot\delta\mathcal{X}_0, \tag{39}$$

where $\delta\mathcal{X}$ is either an infinitesimal perturbation of the original system or a finite solution of the linearized system. Assume perturbations grow like $\delta\mathcal{X}_n\sim\delta\mathcal{X}_{0,n}e^{\lambda_n t}$ along each of the six dimensions. For chaotic systems, the maximum Lyapunov exponent $\lambda>0$ will dominate. Hence, define

$$\lambda=\lim_{t\to\infty}\frac{1}{t}\log\frac{\|\delta\mathcal{X}\|}{\|\delta\mathcal{X}_0\|}=\lim_{t\to\infty}\frac{1}{t}\log\|\delta\mathcal{X}\|, \tag{40}$$

and use Eq. (39) to estimate

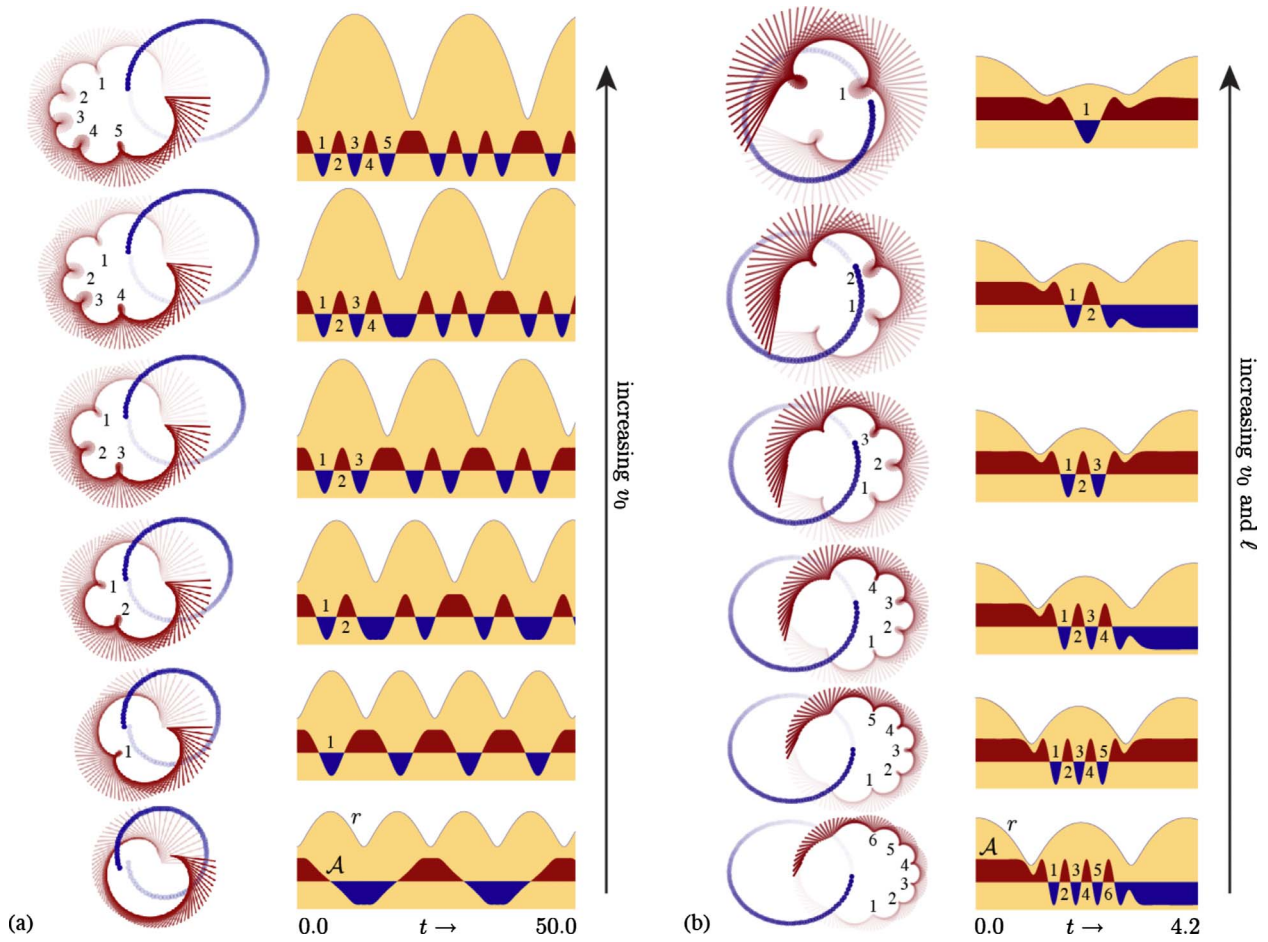

FIG. 12. (Color online) (a) Vertical triangle family of periodic orbits from Fig. 9, including inertial reference frame fading strobe sequence for one revolution (left) and separation r and alignment $\mathcal{A}$ as a function of time t (right). (b) Diagonal disk periodic family of orbits from Fig. 9, including fading strobe sequence (left) and separation r and alignment $\mathcal{A}$ as a function of time t (right). Each successive orbit contains an extra rotation per revolution (spin per orbit).

$$\lambda \sim \frac{1}{t}\log\left\|\frac{\partial \mathcal{X}}{\partial \mathcal{X}_0}\cdot \delta\mathcal{X}_0\right\|, \tag{41}$$

for sufficiently large t. Accomplish this by concurrently numerically integrating the six equations of Eq. (37) and the $6\times 6=36$ equations of Eq. (38).

We check that λ is roughly constant over initial angles and set $\varphi_0=\pi/4$ (with $r_0=1$) to avoid the numerical instabilities in the variational equations at the pointing condition $\varphi_0=\pi/2$. We integrate for 100 periods and apply the Eq. (41) estimate to obtain λ.

Figure 13 plots maximum Lyapunov exponent λ (terrain colors) as a function of initial speed v_0, initial spin ω_0, and slash length $\ell=2R$, in two different cross sections. White represents collisions. Near the synchronous orbit, in the "valley of stability," chaos is absent (blues). Elsewhere near the synchronous frequency $\omega_0=\sqrt{2}$, chaos is strong for small initial speeds $v_0<v_\odot$ (light browns), as the system begins at apopapsis and contracts to peripasis, while the gravity gradient increases; chaos is weak for large initial speeds $v_0>v_\odot$ (yellows and greens), as the system begins at periapsis and expands to apopapsis, while the gravity gradient decreases. Far from synchronous orbit, large positive spin or negative spin are not chaotic (blues), corresponding to the spin-stabilized striped patterns in Figs. 9 and 10.

F. Spin-orbit coupling

The slash-dot body problem facilitates study of the interplay between rotation (spin) and revolution (orbit) in the interaction of physical bodies like asteroids and moonlets. The corresponding two or three body problems, which involve point masses, exhibit revolution but not rotation. The rotation of the slash about its center can be a source or sink of energy and angular momentum that can even unbind the system in cases where corresponding point masses would remain bound.

Given an initial position $\vec{r}_0=-\hat{y}r_0$, initial velocity $\vec{v}_0=-\hat{x}v_0$, initial angle $\varphi_0=\pi/2$, initial spin $\vec{\omega}_0=-\hat{z}\omega_0$, then the constant energy surfaces are ellipses in the $\{\omega_0,v_0\}$ plane,

$$E=T_{\mathcal{O}}+T_{\mathcal{S}}+V=\frac{1}{2}\mu v_0^2+\frac{1}{6}m_sR^2\omega_0^2-\frac{Gm_sm_d}{2R}\log\left[\frac{r_0+R}{r_0-R}\right], \tag{42}$$

where direct integration provides the potential energy expression in this special parallel case.

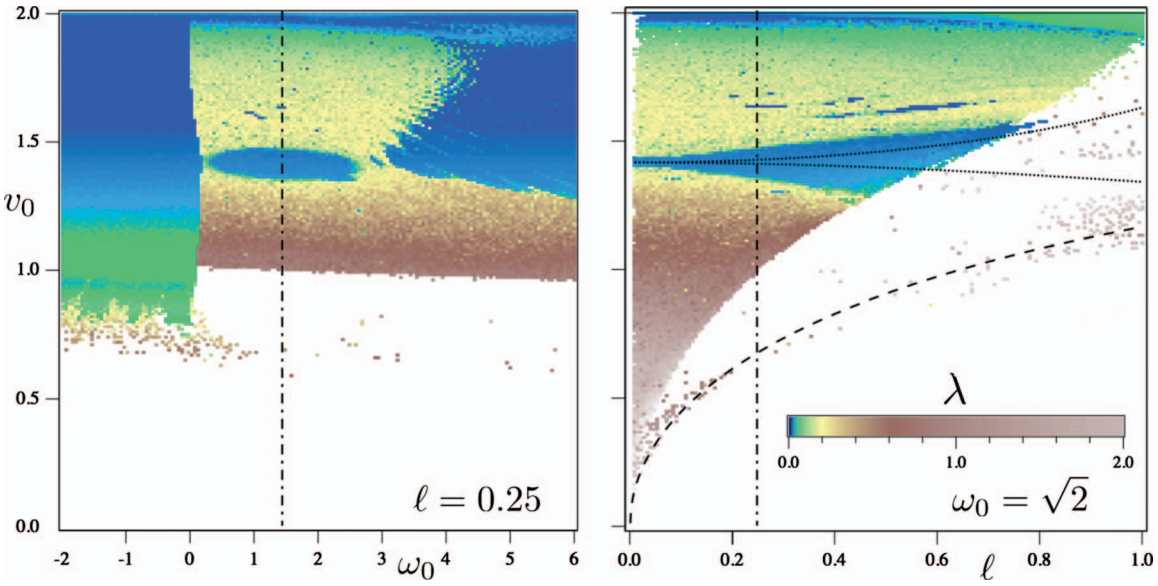

FIG. 13. (Color) Terrain colors represent estimates of the maximum Lyapunov exponent λ as a function of the initial speed v_0, initial spin ω_0, and slash length ℓ. White represents collisions. Near the synchronous orbit, at $v_0=\sqrt{2}=\omega_0$, chaos is absent (blues). Elsewhere near the synchronous frequency $\omega_0=\sqrt{2}$, chaos is weak for large initial speeds $v_0>v_\odot$ (yellows and greens) and strong for small initial speeds $v_0<v_\odot$ (light browns). Far from synchronous orbit, in a kind of gyroscopic stabilization, large positive spin or negative spin are not chaotic (blues). Vertical dot-dash lines indicate the intersection of the two plots.

The $E=0$ contour is the perimeter of the dark gray ellipse in the inset to Fig. 14. The light gray rectangle surrounding the ellipse is the region of initial velocities for which point particles are bound but the slash and dot may be unbound; here, total energy is positive, but only when including the spin kinetic energy $T_\mathcal{S}$. The black point in this region indicates the initial velocities of the corresponding time series.

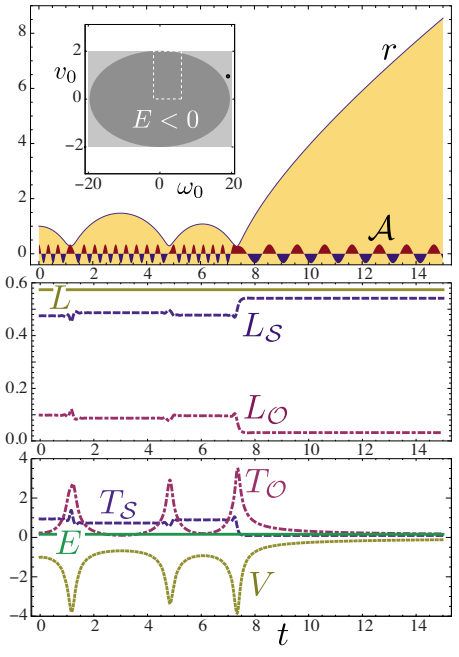

FIG. 14. (Color online) Spin-orbit coupling can unbind the slash and dot. Displacement r and alignment $\mathcal{A}$ as a function of time t (top graph) for initial speed $v_0=0.95$ and initial spin $\omega_0=19$ (inset's black point) and slash length $\ell=0.25$. Angular momentum $L=L_\mathcal{S}+L_\mathcal{O}$ (middle graph) and energy $E=T_\mathcal{S}+T_\mathcal{O}+V$ (bottom graph) remain constant but redistribute from spin to orbit at the close encounter near time $t=7$.

The top graph in Fig. 14 plots separation r and alignment $\mathcal{A}$ versus time. After two bound orbits, near the periapsis at about $t=7$, the slash's spin suddenly decreases and the orbit of the system consequently expands to infinity. The middle-graph depicts the accompanying transfer or redistribution of angular momentum $L=L_\mathcal{S}+L_\mathcal{O}$, and the bottom graph depicts the redistribution of energy $E=T_\mathcal{S}+T_\mathcal{O}+V$ between spin and orbit.

Such interactions may be important in understanding the escape rates of asteroids from asteroid belts or ring systems. The inverse process, which we also observe, in which the slash spin suddenly increases and the orbit consequently shrinks, may help explain the anomalous rotation rates of some asteroids that have been spun up to near disruption.

IV. CONCLUSIONS

The title of George Gamow's famous book, *One Two Three…Infinity* [22] suggests the gap between the two body problem that Newton solved exactly and the three body problem for which Newton wrote [23] "my head never ached but with my studies of the Moon [and Earth and Sun]." The slash-dot body problem lies somewhere in between, perhaps closer to the two body problem in terms of its definition, but definitely closer to the three body problem in terms of the infinite richness of its solutions.

As we demonstrate here, the force and torque in the slash-dot body problem yield compact algebraic expressions whose nonlinearity still enables arbitrarily complicated

orbits. This—perhaps unexpected—simplification greatly facilitates both analytic and numerical analysis. Families of periodic orbits coexist with generic chaotic orbits.

The slash-dot body problem is also a superb prototype for the study of rotation and revolution. Points cannot rotate, but line segments can. This is an especially simple system in which to study the interplay of rotation and revolution. It is a reminder that not everything can be well approximated as a point, and its details, like the effective moment arm in Fig. 5, help to break bad habits and develop good intuition about the full body problem.

In addition, the dynamics of the slash and dot are especially beautiful, in a way that is difficult to convey on the static page. We have attempted to communicate the graceful pirouettes of this pas de deux in the three-dimensional strobed orbit of Fig. 2, and the two-dimensional strobed orbits of Fig. 12, as well as in online animations [14].

Extensions to the slash-dot body problem include relaxing the initial conditions to allow orbits out of the plane, where the interplay between spin and orbit, rotation and revolution, is even richer. Additional cases of the full body problem that might feature integrable forces and torques include the interaction of two line segments, the slash-slash (//) body problem.

ACKNOWLEDGMENTS

This research was supported by NSF Grant No. DMR-0649112 and The College of Wooster. J. F. L. thanks B. J. Breen for helpful discussions and the University of Portland for its hospitality and the use of its computer cluster.

[1] H. Poincaré, *New Methods of Celestial Mechanics* (American Institue of Physics, New York, 1993); *Les Méthodes Nouvelles de la Mécanique Céleste* (Gauthier-Villars, Paris, 1892, 1893, 1899).
[2] M. C. Gutzwiller, Rev. Mod. Phys. **70**, 589 (1998).
[3] C. Marchal, *Three-Body Problem* (Elsevier, Amsterdam, 1990).
[4] M. Valtonen and H. Karttunen, *The Three-Body Problem* (Cambridge University Press, Cambridge, 2006).
[5] J. Nagler, Phys. Rev. E **71**, 026227 (2005).
[6] N. J. Harmon, C. Leidel, and J. F. Lindner, Am. J. Phys. **71**, 871 (2003).
[7] J. F. Lindner, M. I. Roseberry, D. E. Shai, N. J. Harmon, and K. D. Olaksen, Int. J. Bifurcat. Chaos **18**, 455 (2008).
[8] J. C. Sprott, Am. J. Phys. **77**, 783 (2009).
[9] C. Moore, Phys. Rev. Lett. **70**, 3675 (1993).
[10] A. Chenciner and R. Montgomery, Ann. Math. **152**, 881 (2000).
[11] T. Lee, M. Leok, and N. H. McClamroch, Celest. Mech. Dyn. Astron. **98**, 121 (2007).
[12] J. Wisdom, S. J. Peale, and F. Mignard, Icarus **58**, 137 (1984).
[13] N. Giordano and H. Nakanishi, *Computational Physics 2/E* (Addison-Wesley, 2006).
[14] See supplementary material at http://link.aps.org/supplemental/10.1103/PhysRevE.81.036208 for QuickTime animations of the slash-dot system.
[15] Ch. Jaffé, S. D. Ross, M. W. Lo, J. Marsden, D. Farrelly, and T. Uzer, Phys. Rev. Lett. **89**, 011101 (2002).
[16] S. G. Love and T. J. Ahrens, Nature (London) **386**, 154 (1997).
[17] W. H. Press, S. A. Teukolsky, W. T. Vetterling, and B. P. Flannery, *Numerical Recipes in C: The Art of Scientific Computing* (Cambridge University Press, Cambridge, England, 1992).
[18] S. D. Cohen and A. C. Hindmarsh, Comput. Phys. **10**, 138 (1996).
[19] Wolfram Research, Inc., Mathematica, Version 7.0 (Champaign, Illinois, 2008).
[20] R. Abraham and J. E. Marsden, *Foundations of Mechanics* (Benjamin/Cummins, Reading, MA, 1978).
[21] T. S. Parker and L. O. Chua, *Practical Numerical Algorithms for Chaotic Systems* (Springer-Verlag, New York, 1989).
[22] G. Gamow, *One Two Three… Infinity: Facts and Speculations of Science* (Dover, New York, 1988).
[23] V. G. Szebehely and H. Mark, *Adventures in Celestial Mechanics* (Wiley, New York, 1998).